

Interchannel coupling in Auger decay processes: Characterization of normal and satellite lines in the Auger electron spectrum of the LiF molecule

Renato Colle and Stefano Simonucci
Scuola Normale Superiore, 56100 Pisa, Italy
(Received 26 March 1990)

An alternative method for taking into account correlation effects in the calculation of Auger decay rates is presented here. This approach, which generalizes a technique recently proposed by the authors [Phys. Rev. A **39**, 6247 (1989)], is based on the coupling of final ionic states and decay channels and has been applied to the construction of a "theoretical" Auger spectrum of the LiF molecule in which transitions also due to shakeoff and shakeup processes are taken into account.

I. INTRODUCTION

In a series of papers¹⁻³ we have proposed a new method for calculating partial and total decay rates and also resonance energies on atomic or molecular Auger emission processes. This approach, which is extensively described in Ref. 1 hereafter referred to as I, is characterized by two main advantages. First, it can be easily applied to any type of molecule with a computational effort of the same order of magnitude as a standard bound-state calculation. This peculiarity follows from the fact that the method is based on the expansion in terms of basis functions both of the orbitals and of the effective potential used for their construction. Second, it can be utilized also for the quantitative prediction of other properties; for example, photoionization probabilities or scattering cross sections, and in general in those problems which involve one free electron moving in the field of an atom or molecule.

On the other hand, the main limitation of the method is that each decay channel is treated separately and described by a Hartree-Fock wave function so that the electronic correlation effects are neglected (apart from those introduced by the antisymmetrization of the wave functions). As regards these effects, it is well known that one can distinguish in general between the so-called "short-range" or "dynamic" correlation effects—an efficient description of which requires the presence of the interelectronic coordinates in the wave function—and the "long-range" or "static" correlation effects—those owing to the presence of quasidegeneracies among different independent particle states (see, e.g., Ref. 4). In particular, one usually distinguishes among three main ways through which the electron correlation may enter into the calculation of the Auger transition rates: (1) the electron correlation in the initial state of the singly ionized target (CIS); (2) the electron correlation in the final ionic states of the doubly ionized target (CFIS); and (3) the electron correlation in the final states of the complete system (CFS).

In their calculations of the *K-LL* Auger decay rates of the neon atom Kelly⁵ and Howat, Aberg, and Goscinski⁶ showed that the inclusion of correlation effects greatly improves the quality of the theoretical results and more

specifically that while CFS are as important as CFIS, both are appreciably more important than CIS. Calculation of the same degree of accuracy, however, has not been possible on molecules, up to now, because of the polycentric nature of the system that hinders the use of numerical techniques utilized also by Kelly and Howat.

In this article we improve our method which allows evaluation of Auger decay rates also in molecules by taking explicitly into account "static" correlation effects, that is, by including both CFIS and CFS effects through the coupling of the Hartree-Fock wave functions which describe the various ionic states and decay channels. This result is achieved by solving a time-independent Schrödinger equation relative to a Hamiltonian that is the *N*-particle generalization of the Hartree-Fock operator used in I for the construction of the continuum orbitals and characterized by the presence of a potential projected into a finite discrete basis set of L^2 functions. The application of our method to specific problems, like the Auger spectrum of the Ne and LiF, shows that the inclusion of the interchannel coupling largely improves the quality of the results obtained in previous papers^{1-3,7} in which the various decay channels were treated separately.

The outline of this paper is the following. In Sec. II we describe our method. In Sec. III we apply it to the evaluation of the decay rates and resonance energies of the Auger spectrum of the neon atom to compare our results with those obtained by Kelly⁵ and Howat, Aberg, and Goscinski.⁶ In the same section, we also present a "theoretical" Auger spectrum of the LiF molecule in which secondary transitions, produced by shakeup or shakeoff processes, are taken into account, and we compare this spectrum with the experimental one.

II. METHOD

In this section we develop a method for studying the Auger effect interpreted as a two-step process in which the decay can be treated separately from the initial ionization and in which the resonance originates from the interaction between the quasibound state of the initial ion and the continua of the doubly ionized target. These as-

sumptions are in general appropriate for interpreting many Auger spectra of atoms or molecules where the resonances are widely spaced and not too close to the double ionization threshold so that one can neglect the interaction between the primary fast electron and the Auger electron: this means disregarding the so-called post collisional effects.⁸

In particular, since we are mostly interested in the decay part of the process we can study this problem as a particular example of autoionization in a system that has been previously ionized, and therefore use for its interpretation the theory developed by Fano⁹ for treating autoionizing states, as done also by Howat, Aberg, and Gosinski⁶ for the Auger effect in atoms.

A. Fano's theory

Let us start considering the internal structure of the wave function $\Psi_{\alpha,\epsilon}^-$ that describes the $(N-1)$ -electron system produced by the initial single ionization. We impose to $\Psi_{\alpha,\epsilon}^-$ the ingoing wave boundary condition, since we are interested in the probability distribution of the various entrance channels for an Auger electron escaping into a given channel α with kinetic energy \mathcal{E} measured from the threshold energy E_α . Since we are interested in a problem where an isolated resonance state $|\Phi\rangle$ interacts with N_c continua, using Fano's theory and the formalism of Ref. 10, we represent $\Psi_{\alpha,\epsilon}^-$ in terms of a configuration interaction expansion of the type

$$\Psi_{\alpha,\epsilon}^- = a_\alpha^-(\mathcal{E})\Phi + \sum_{\beta=1}^{N_c} \int_0^\infty \chi_{\beta,\tau}^- C_{\beta,\alpha}^-(\tau, \mathcal{E}) d\tau, \quad (1)$$

with the normalization condition

$$\langle \Psi_{\alpha,\epsilon}^- | \Psi_{\beta,\epsilon'}^- \rangle = \delta_{\alpha\beta} \delta(E_\alpha + \mathcal{E} - E_\beta - \mathcal{E}'). \quad (2)$$

In Eq. (1) $\chi_{\beta,\tau}^-$ is a continuum function representing a direct scattering channel, the asymptotic behavior of which is given by

$$\lim_{r \rightarrow \infty} \chi_{\beta,\tau}^- = \sum_{\gamma=1}^{N_c} \frac{\Omega_\gamma}{2ir} (e^{i\theta_\gamma(\tau,r)} \delta_{\gamma\beta} - e^{-i\theta_\gamma(\tau,r)} S_{\gamma\beta}^+). \quad (3)$$

The symmetry-adapted wave functions $\{\Omega_\gamma\}$ describe possible states of the doubly ionized target and contain also the angular coordinates of the outgoing electron. Its radial phase $\theta_\gamma(\tau, r)$ in the channel γ depends on the nature of the long-range interaction.

To determine the expansion coefficient in Eq. (1) without any loss of generality, one can assume that the channel functions $\{\chi_{\beta,\tau}^-\}$ do not interact among themselves. This means that they have been obtained from a given set of interacting continuum functions $\{\chi_{\beta,\epsilon}\}$ through the diagonalization of the corresponding Hamiltonian matrix:

$$\langle \chi_{\beta,\epsilon} | H - E | \chi_{\gamma,\epsilon'} \rangle = (E_\beta + \epsilon - E) \delta(E_\beta + \epsilon - E_\gamma - \epsilon') + V_{\beta\gamma}(\epsilon, \epsilon'; E). \quad (4)$$

Note that from the solution of this set of equations one derives also the expression of the scattering matrix S

whose adjoint is used in Eq. (3).

The expansion coefficients in Eq. (1) can be determined by requiring that

$$\langle \Phi | H - E | \Psi_{\alpha,\epsilon}^- \rangle = \langle \chi_{\beta,\epsilon}^- | H - E | \Psi_{\alpha,\epsilon}^- \rangle = 0 \quad (5)$$

and solving the following system of equations obtained under the assumption of noninteracting channels:

$$(E_\Phi - E) a_\alpha^-(\mathcal{E}) + \sum_{\beta=1}^{N_c} \int_0^\infty M_\beta^-(\tau, \mathcal{E}) C_{\beta\alpha}^-(\tau, \mathcal{E}) d\tau = 0, \quad (6a)$$

$$a_\alpha^-(\mathcal{E}) M_\beta^-(\epsilon, \mathcal{E})^* + (\epsilon + E_\beta - E) C_{\beta\alpha}^-(\epsilon, \mathcal{E}) = 0, \quad (6b)$$

with

$$M_\beta^-(\epsilon, \mathcal{E}) = \langle \Phi | H - E | \chi_{\beta,\epsilon}^- \rangle, \quad (E_\Phi - E) = \langle \Phi | H - E | \Phi \rangle. \quad (7)$$

The solution of this set of equations can be carried out using the same technique proposed by Fano⁹ to remove the singularity at $E = E_\beta + \epsilon$. This leads to the following expression for $\Psi_{\alpha,\epsilon}^-$ in Eq. (1):

$$\Psi_{\alpha,\epsilon}^- = \chi_{\alpha,\epsilon}^- + \frac{M_\alpha^-(\mathcal{E}, \mathcal{E})}{E - E_\alpha - i\frac{\Gamma}{2}} \times \left[\Phi + \lim_{\nu \rightarrow 0} \sum_{\beta=1}^{N_c} \int_0^\infty \frac{\chi_{\beta,\tau}^- M_\beta^-(\tau, \mathcal{E})^*}{E - E_\beta - \tau - i\nu} d\tau \right], \quad (8)$$

with the quantities Γ and E_r defined as

$$\Gamma = \sum_{\beta=1}^{N_c} \Gamma_\beta^- = 2\pi \sum_{\beta=1}^{N_c} |M_\beta^-(\mathcal{E}, \mathcal{E})|^2, \quad (9)$$

$$E_r = E_\Phi + \Delta, \quad \Delta = \sum_{\beta=1}^{N_c} \mathcal{P} \int_0^\infty \frac{|M_\beta^-(\tau, \mathcal{E})|^2}{E - E_\beta - \tau} d\tau. \quad (10)$$

Equation (10) shows that the resonance energy E_r deviates from that of the quasibound state $|\Phi\rangle$ by the energy shift Δ , which is expressed in terms of the principal part \mathcal{P} of the integrals in Eq. (10). Furthermore, the quantity Γ defined in Eq. (9) can be interpreted as the total Auger decay rate due to the nonradiative transitions from the resonance state $|\Phi\rangle$ and consistently $\Gamma_\beta^- = 2\pi |M_\beta^-(\mathcal{E}, \mathcal{E})|^2$ is the partial, nonradiative decay rate into channel β .

B. Our approach

From Fano's theory for the interaction among discrete and continuum states one obtains general analytical expressions to interpret a typical Auger spectrum in terms of resonance energies and decay probabilities. However, for the effective application of the theory one needs to construct the continuum function (1) as a solution of a time-independent Schrödinger equation relative to a Hamiltonian that represents a physically reasonable approximation of the true molecular one. To this end, we

propose a model Hamiltonian for the electronic part of the problem in which the potential energy operator is substituted by its projection onto a set of m basis functions and the expression of the complete operator in atomic units is given as

$$H(1, 2, \dots, N-1) = \sum_{j=1}^{N-1} [\hat{T}(j) + \hat{V}_{\pi}^{e-n}(j)] + \frac{1}{2} \sum_{i,j=1}^{N-1} \hat{g}_{\pi}(i, j), \quad (11)$$

$$\hat{T}(1) = -\frac{1}{2} \nabla^2(1), \quad (12)$$

$$\hat{V}_{\pi}^{e-n}(1) = \hat{\pi}(1) \hat{V}^{e-n}(1) \hat{\pi}(1), \quad (13)$$

$$\hat{g}_{\pi}(1, 2) = \hat{\pi}(1) \hat{\pi}(2) \hat{g}(1, 2) \hat{\pi}(1) \hat{\pi}(2),$$

$$\hat{\pi}(1) = \sum_{j=1}^m |\psi_j(1)\rangle \langle \psi_j(1)|. \quad (14)$$

In Eq. (13) \hat{V}^{e-n} and \hat{g} are respectively the electron-nuclei and electron-electron potential-energy operators, while $\hat{\pi}$ in Eq. (14) is the projection operator—constructed with the orthonormal basis functions $\{\psi_j\}$ —that, when applied to an N -particle wave function $\Psi(1, \dots, N)$, gives

$$\begin{aligned} \hat{\pi}(j) \Psi(1, 2, \dots, N) \\ = \sum_{k=1}^m \psi_k(j) \int \psi_k(j')^* \Psi(1, 2, \dots, j', \dots, N) dj'. \end{aligned} \quad (15)$$

Note that, if the basis set $\{\psi_j\}$ were complete, the spectrum of the Hamiltonian defined in Eq. (11) would be the same as that of the standard electronic Hamiltonian. However, as done in I, we use a finite basis set containing only L^2 functions that, in our applications, are Hermite Gaussian functions¹¹ with parameters optimized as explained in Sec. III.

Because of this approximation which imposes a short-range character to the electrostatic potential, the eigenfunctions of our model Hamiltonian, belonging to the continuum part of the spectrum, will have an asymptotic behavior governed by the centrifugal potential. Therefore, if one is interested in obtaining the phase shifts of the various decay channels, a matching procedure with the exact long-range solutions of the problem is necessary (see Ref. 2). On the other hand, as far as the Auger matrix elements are concerned, our calculations in I show that the incorrect asymptotic behavior of the continuum orbitals reflects essentially in a small (about 5%) scaling of the Auger matrix elements, that is about the same for all the elements and is due to a small damping of the orbital amplitude.

Since we are not able to obtain the exact solutions of the electronic Hamiltonian, even if projected as done in Eq. (11), we reduce the $(N-1)$ -particle Hilbert space—inside which we look for the best representation of our state—to the space spanned by the following set of functions $\{\chi_{\alpha, \mathbf{k}}\}$:

$$\begin{aligned} \chi_{\alpha, \mathbf{k}}(1, 2, \dots, N-1) \\ = \sqrt{(N-1)} \hat{A}_i [\varphi_{\mathbf{k}}(1) \Theta_{\alpha}(2, \dots, N-1)], \end{aligned} \quad (16)$$

where Θ_{α} is a linear combination of the smallest number of Slater determinants necessary to obtain a symmetry-adapted wave function for the state α of the doubly ionized molecule, while $\varphi_{\mathbf{k}} = \eta_{\mathbf{k}}(\mathbf{r}_1) \sigma(s_1)$ is the spin orbital that represents the Auger electron having asymptotically a kinetic energy equal to $k^2/2$. Finally, in Eq. (16) \hat{A}_i is the idempotent operator that completely antisymmetrizes $\chi_{\alpha, \mathbf{k}}$ by taking into account also the permutations between the Auger electron and those described by the antisymmetrized and normalized wave function Θ_{α} .

Note that in the specific applications of our method $\{\Theta_{\alpha}\}$ represents the finite set of energetically allowed state of the doubly ionized molecule and that, to simplify the treatment, we require the fulfillment of the following orthonormality relations among the various group functions:

$$\langle \Theta_{\alpha}(1, \dots, N-2) | \Theta_{\alpha'}(1, \dots, N-2) \rangle = \delta_{\alpha\alpha'} \forall \alpha, \alpha', \quad (17)$$

$$\langle \Theta_{\alpha}(1, \dots, N-2) | \varphi_{\mathbf{k}}(j) \rangle_j = 0, \quad \forall \alpha, \mathbf{k}, \quad (18)$$

$$\langle \eta_{\mathbf{k}}(\mathbf{r}) | \eta_{\mathbf{k}'}(\mathbf{r}) \rangle = (2\pi)^3 \delta(\mathbf{k} - \mathbf{k}'). \quad (19)$$

It is clear that the more convenient way for taking into account Eq. (17), when Slater determinants are used, is to construct the various functions $\{\Theta_{\alpha}\}$ with orbitals $\{\theta_j\}$ obtained as eigenfunctions of the same effective operator \hat{F} defined as

$$\hat{F} = \hat{h} + \sum_{j=1}^{\text{occ}} a_j (2\hat{J}_j - \hat{K}_j). \quad (20)$$

In Eq. (20) \hat{h} , \hat{J}_j , and \hat{K}_j are, respectively, the mono-electronic, Coulomb, and exchange operators, the latter two of which are constructed with the orbital θ_j whose occupation number, averaged over all the final ionic states $\{\Theta_{\alpha}\}$, is a_j .

The preliminary step of our method thus requires the self-consistent-field (SCF) determination of the eigenfunctions of the average Hartree-Fock operator defined in Eq. (20). These eigenfunctions, in our applications, will be expressed as linear combinations of a finite set of Hermite Gaussian functions of any order and position.

In a similar way, to satisfy relation (18), we require that $\eta_{\mathbf{k}}$ be orthogonal to all the occupied orbitals $\{\theta_j\}$ that have been used for the construction of the final ionic states $\{\Theta_{\alpha}\}$. Furthermore, since $\eta_{\mathbf{k}}$ must be an asymptotic eigenfunction of the kinetic energy operator \hat{T} [see Hamiltonian (11)] we obtain its analytic expression by solving

$$\hat{T}_q \eta_{\mathbf{k}} = \frac{k^2}{2} \eta_{\mathbf{k}}, \quad \hat{T}_q = (1 - \hat{P}) \hat{T} (1 - \hat{P}) = \hat{T} + \hat{V}_{\text{PK}}, \quad (21)$$

where

$$\hat{V}_{\text{PK}} = -\hat{P} \hat{T} - \hat{T} \hat{P} + \hat{P} \hat{T} \hat{P}, \quad \hat{P} = \sum_j^{\text{occ}} |\theta_j\rangle \langle \theta_j|. \quad (22)$$

In Eq. (21) \hat{V}_{PK} is a Phillips-Kleiman operator¹² that allows us to take into account the orthogonality relations $\{\langle \theta_j | \eta_{\mathbf{k}} \rangle = 0\}$ for each occupied orbital and \hat{P} the corre-

sponding projection operator.

The solution of Eq. (21) is simply given by

$$\eta_{\mathbf{k}}(\mathbf{r}) = e^{i\mathbf{k}\cdot\mathbf{r}} + \hat{G}_0(k)\hat{t}(k)e^{i\mathbf{k}\cdot\mathbf{r}}, \quad (23)$$

where $\hat{G}_0(k) = (k^2/2 - \hat{T})^{-1}$ is the free-particle Green function and $\hat{t}(k)$ the transition operator defined by

$$\hat{t}(k) = \hat{V}_{\text{PK}} + \hat{V}_{\text{PK}}\hat{G}_0(k)\hat{t}(k). \quad (24)$$

Since we are interested in the representation of $\hat{t}(k)$ inside a space defined by a finite set of basis functions, as long as $[\hat{V}_{\text{PK}} - \hat{V}_{\text{PK}}\hat{G}_0(k)\hat{V}_{\text{PK}}]$ can be inverted, Eq. (24) becomes a matrix equation with solution

$$t(k) = \underline{V}_{\text{PK}} \frac{1}{\underline{V}_{\text{PK}} - \underline{V}_{\text{PK}}\underline{G}_0(k)\underline{V}_{\text{PK}}} \underline{V}_{\text{PK}}. \quad (25)$$

Note that in Refs. 2, 13, and 14 we have derived general expressions for the integrals required in Eq. (25) and in the other equations of the article when the basis set is constituted by Hermite Gaussian functions of any order and position.

Having solved the Hartree-Fock equations for the occupied orbitals $\{\theta_j\}$ and Eq. (21) for the continuum orbital $\eta_{\mathbf{k}}$, we are able to construct the $(N-1)$ -particle wave functions defined in Eq. (16) that constitute the initial set of interacting channels and are analogous to the continuum functions $\{\chi_{\beta,\epsilon}\}$ given in Eq. (4). Because of the orthonormality relations (17)–(19), one obtains the following expression for the Hamiltonian matrix element between two interacting channels.

$$\begin{aligned} \langle \chi_{\alpha,\mathbf{k}} | \hat{H}(1, \dots, N-1) | \chi_{\alpha',\mathbf{k}'} \rangle \\ = (2\pi)^3 \delta(\mathbf{k} - \mathbf{k}') [(k^2/2)\delta_{\alpha\alpha'} + H_{\alpha\alpha'}^{N-2}] \\ + \langle \varphi_{\mathbf{k}} | \hat{V}_{\pi}^{e-n} + \hat{W}_{\pi}^{\alpha\alpha'} | \varphi_{\mathbf{k}'} \rangle, \end{aligned} \quad (26)$$

with

$$H_{\alpha\alpha'}^{N-2} = \langle \Theta_{\alpha} | \hat{H}(1, \dots, N-2) | \Theta_{\alpha'} \rangle \quad (27)$$

and

$$\begin{aligned} \hat{W}_{\pi}^{\alpha\alpha'}(1) = \sum_{l=2}^{N-1} \langle \Theta_{\alpha}(2, \dots, N-1) | \hat{g}_{\pi}(1, l) (1 - \hat{P}_{1l}) \\ \times | \Theta_{\alpha'}(2, \dots, N-1) \rangle. \end{aligned} \quad (28)$$

In Eq. (27) \hat{H} is the $(N-2)$ -particle Hamiltonian defined as in Eq. (11) and \hat{P}_{1l} the operator that interchanges the $(1, l)$ variables.

Equation (26) suggests that the second step in our process should be the diagonalization of the matrix \underline{H}^{N-2} constructed with the wave functions of the doubly ionized target. This step allows us to introduce correlation contributions (CFIS) owing to interactions among final ionic states, and simultaneously, to obtain upper bounds to the exact eigenvalues of the $(N-2)$ -electron Hamiltonian.

By indicating with $\{E_{\alpha}\}$ and $\{\hat{\Theta}_{\alpha}\}$, respectively the eigenvalues and eigenvectors of \underline{H}^{N-2} , and with $\{\tilde{\chi}_{\alpha,\mathbf{k}}\}$ the partially correlated wave functions, defined as in Eq. (16) but with Θ_{α} substituted by $\hat{\Theta}_{\alpha}$, we have

$$\begin{aligned} \langle \tilde{\chi}_{\alpha,\mathbf{k}} | \hat{H}(1, \dots, N-1) | \tilde{\chi}_{\alpha',\mathbf{k}'} \rangle \\ = (2\pi)^3 \delta(\mathbf{k} - \mathbf{k}') \delta_{\alpha\alpha'} \left[\frac{k^2}{2} + E_{\alpha} \right] \\ + \langle \varphi_{\mathbf{k}} | \hat{V}_{\pi}^{e-n} + \hat{W}_{\pi}^{\alpha\alpha'} | \varphi_{\mathbf{k}'} \rangle, \end{aligned} \quad (29)$$

where $\hat{W}_{\pi}^{\alpha\alpha'}$ is the analog of the matrix element (28) taken between $\hat{\Theta}_{\alpha}$ and $\hat{\Theta}_{\alpha'}$.

For obtaining the final noninteracting channels that correspond to the functions $\{\chi_{\alpha,\epsilon}\}$ used in Eq. (1), we have to solve the Schrödinger equation for the Hamiltonian (11) projected into the space of the orthonormal functions $\{\tilde{\chi}_{\alpha,\mathbf{k}}\}$; this means

$$\hat{\mathcal{H}} | \chi_{\alpha,E}^- \rangle = E | \chi_{\alpha,E}^- \rangle, \quad (30)$$

with

$$\hat{\mathcal{H}} = \hat{\mathcal{H}}_0 + \hat{\mathcal{V}}, \quad (31)$$

$$\hat{\mathcal{H}}_0 = \sum_{\beta}^{\text{occ}} \int \frac{d\mathbf{k}}{(2\pi)^3} | \tilde{\chi}_{\beta,\mathbf{k}} \rangle \left[\frac{k^2}{2} + E_{\beta} \right] \langle \tilde{\chi}_{\beta,\mathbf{k}} |, \quad (32)$$

$$\begin{aligned} \hat{\mathcal{V}} = \sum_{\beta,\beta'}^{\text{occ}} \int \frac{d\mathbf{k}}{(2\pi)^3} \int \frac{d\mathbf{k}'}{(2\pi)^3} | \tilde{\chi}_{\beta,\mathbf{k}} \rangle \langle \varphi_{\mathbf{k}'} | \\ \times \hat{V}_{\pi}^{e-n} + \hat{W}_{\pi}^{\beta\beta'} | \varphi_{\mathbf{k}'} \rangle \langle \tilde{\chi}_{\beta',\mathbf{k}'} |. \end{aligned} \quad (33)$$

Using the ingoing wave boundary condition, the solution of Eq. (30), which corresponds to an Auger electron escaping into channel α with kinetic energy $k^2/2$, can be written as follows:

$$| \chi_{\alpha,E}^- \rangle = | \tilde{\chi}_{\alpha,\mathbf{k}} \rangle + \hat{G}_0^-(E) \hat{T}^-(E) | \tilde{\chi}_{\alpha,\mathbf{k}} \rangle, \quad E = E_{\alpha} + \frac{k^2}{2}, \quad (34)$$

where

$$\hat{G}_0^-(E) = \lim_{\epsilon \rightarrow 0} \sum_{\beta}^{\text{occ}} \int \frac{d\mathbf{k}}{(2\pi)^3} \frac{| \chi_{\beta,\mathbf{k}} \rangle \langle \tilde{\chi}_{\beta,\mathbf{k}} |}{(E - E_{\beta}) - k^2/2 - i\epsilon} \quad (35)$$

is the Green function relative to $\hat{\mathcal{H}}_0$ and $\hat{T}^-(E)$ the $(N-1)$ -particle transition operator defined by

$$\hat{T}^-(E) = \hat{\mathcal{V}} + \hat{\mathcal{V}} \hat{G}_0^-(E) \hat{T}^-(E). \quad (36)$$

We observe that, because of Eqs. (13), (33), and (36), both the operators $\hat{\mathcal{V}}$ and $\hat{T}^-(E)$ are defined inside a space that has the identity $\hat{\mathcal{J}}$ given by

$$\hat{\mathcal{J}}(1, 2, \dots, N-1) = \hat{\pi}(1)\hat{\pi}(2) \cdots \hat{\pi}(N-1), \quad (37)$$

with $\hat{\pi}$ the projection operator defined in Eq. (14). It follows that as long as $[\hat{\mathcal{V}} - \hat{\mathcal{V}}\hat{G}_0(E)\hat{\mathcal{V}}]$ can be inverted, the matrix representation of $\hat{T}^-(E)$ inside this space is given by

$$\underline{T}^-(E) = \underline{\mathcal{V}} \frac{1}{\underline{\mathcal{V}} - \underline{\mathcal{V}}\underline{G}_0(E)\underline{\mathcal{V}}} \underline{\mathcal{V}}. \quad (38)$$

Analogously, we observe that from Eq. (34) one can project out an orbital $\eta_{\mathbf{k},\alpha}^-(\mathbf{r})$, which represents the component into channel α of the continuum function for the Auger electron:

$$\begin{aligned}
|\eta_{k,\alpha}^- \rangle &= \langle \sqrt{N-1} \hat{A}_t \{ \tilde{\Theta}_{\alpha} \sigma \} | \chi_{\alpha,E}^- \rangle \\
&= |\eta_k \rangle + \lim_{\epsilon \rightarrow 0} \int \frac{d\mathbf{k}'}{(2\pi)^3} \frac{|\eta_k \rangle \langle \eta_k | \hat{\tau}_{\alpha}(E) | \eta_k \rangle}{(E - E_{\alpha}) - k'^2/2 - i\epsilon},
\end{aligned} \quad (39)$$

where

$$\hat{\tau}_{\alpha}(E) = \langle (N-1) \hat{A}_t \{ \tilde{\Theta}_{\alpha} \sigma \} | \hat{T}^{-}(E) | \tilde{\Theta}_{\alpha} \sigma \rangle \quad (40)$$

and σ is the spin function for the Auger electron. Equation (39), which is the analog for the outgoing electron of Eq. (34) for the $(N-1)$ -particle wave function, can be written

$$|\eta_{k,\alpha}^- \rangle = |\eta_k \rangle + \hat{g}_{\alpha}^{-}(E) \hat{\tau}_{\alpha}(E) |\eta_k \rangle, \quad (41)$$

where

$$\hat{g}_{\alpha}^{-}(E) = \lim_{\epsilon \rightarrow 0} \int \frac{d\mathbf{k}}{(2\pi)^3} \frac{|\eta_k \rangle \langle \eta_k |}{(E - E_{\alpha}) - k^2/2 - i\epsilon} \quad (42)$$

is the free-particle Green function defined in a space orthogonal to that of the occupied orbitals $\{\theta_j\}$.

To conclude this section, we point out that, according to Eqs. (7) and (9) of Sec. II A, the partial and total Auger decay rates relative to the initial state $|\Phi\rangle$ can be calculated from the matrix elements $\{M_{\alpha}^{-} = \langle \Phi | H - E | \chi_{\alpha,E}^- \rangle\}$ for the various decay channels α , while the energy shift Δ can be obtained using Eq. (10) of Sec. II A.

As far as the matrix elements $\{M_{\alpha}^{-}\}$ are concerned, we observe that, since the initial-state wave function Φ is entirely contained into a L^2 space, usually the same as that of the identity operator \hat{J} in Eq. (37), one can project also the wave function $\chi_{\alpha,E}^-$ into this space, and then utilize for $\hat{G}_{\alpha}^{-}(E)$ in Eq. (35) its matrix representation into this space. The price to be paid for this projection is that we lose the components of

$$\sum_{j=1}^{N-1} \hat{T}(j) \Phi(1, \dots, N-1)$$

that lie outside this space: such components, however, give contributions to M_{α}^{-} which are usually negligible, as shown by our calculations in I.

Finally, as long as the energy shift Δ is concerned, we observe that, using our scheme, we do not need to perform the principal part integration required in Eq. (10), but, as explained in Ref. 3, the value of Δ can be simply obtained through the evaluation of the real part of the Green function (35) represented in the space of the identity operator \hat{J} .

III. CALCULATION OF ATOMIC AND MOLECULAR SPECTRA

A. Ne atom

As done in I, we test our coupled-channel approach on the K -LL Auger spectrum of the neon atom, comparing our results with those obtained by Kelly⁵ and Howat, Aberg, and Goscinski,⁶ through different procedures which are able to take into account correlation contribu-

tions to the Auger matrix elements, but cannot be easily applied to molecular systems.

In our calculations we have used the same basis set ($17s + 11p + 7d$ Hermite Gaussian functions) both for the projected potential in Eq. (11) and for the expansion of the wave functions. The orbital exponents have been chosen through a scaling procedure that allows us to obtain eigenvectors of the average Hartree-Fock operator (20) at energies near to those of the Auger electron in the decay channels. As shown in Table I, these eigenvectors are the most important in the expansion of the continuum orbitals, and therefore, their presence in the initial basis set is an essential prerequisite that can be used as a criterion for the choice of the basis functions (see also procedures suggested in I).

The energy of the initial state described by a separately optimized Hartree-Fock wave function and those of the final ionic states, represented by coupled-channel wave functions constructed with the eigenvectors of the average Hartree-Fock operator (20), are reported in Table II and compared with those obtained from independent-channel calculations and with the experimental quantities.

In Table III(a) we present the absolute values of the partial and total Auger decay rates and in Table III(b), the corresponding relative quantities. The decay probabilities have been calculated starting from an initial state described either by a one-configuration wave function or by the following multiconfiguration-self-consistent-field (MC-SCF) wave function:

$$\begin{aligned}
\Psi(1s^{-1}) &= |1s^1(c_1 2s^2 + c_2 3s^2)2p^6| \\
&\quad + c_3 |1s^2 2s^1 2p^6| + c_4 |1s^1 2s^2 \varphi_p^6|,
\end{aligned} \quad (43)$$

with

$$\begin{aligned}
\varphi_p^6 &= [(2p_0 \bar{3}p_0 + 3p_0 \bar{2}p_0)2p_{-1}^2 2p_1^2] \\
&\quad + [(2p_1 \bar{3}p_1 + 3p_1 \bar{2}p_1)2p_{-1}^2 2p_0^2] \\
&\quad + [(2p_{-1} \bar{3}p_{-1} + 3p_{-1} \bar{2}p_{-1})2p_0^2 2p_1^2].
\end{aligned} \quad (44)$$

Note that in the calculation of the matrix elements one has to take into account that the orbitals of the initial state are nonorthogonal to those of the final states since they have been obtained through different SCF processes.

The results from the coupled channel approach and relative to the uncorrelated initial state include CFIS and CFS contributions that represent the main corrections to the independent-channel results. This allows us to reproduce quite well the experimental quantities even if the number of channels included in the calculations is very small. The use of a partially correlated initial state changes the results only a little (about 2%). These two facts confirm that CIS effects are appreciably less important than CFIS and CFS, as already pointed out by Kelly,⁵ but are much more difficult to take into account through a slowly convergent expansion of the type given in Eq. (43).

As regards the partial decay rates obtained from independent-channel calculations, we observe that their values reported in Table III(a) are smaller by about 10%

TABLE I. Moduli of the expansion coefficients $\{c_j\}$ of the continuum orbitals over the eigenfunctions of the average Hartree-Fock operator defined in Eq. (20). The $\{\epsilon_j\}$ are the corresponding eigenvalues to be compared with the kinetic energy ($k^2/2$) of the Auger electron on each decay channel. The continuum orbitals have been arbitrarily normalized to 1 and the channels classified according to the hole configuration of the final ionic state. All the quantities are given in atomic units.

$^1S(2s^{-1}2s^{-1})$ $k^2/2=27.449\ 11$		$^1S(2p^{-1}2p^{-1})$ $k^2/2=29.438\ 36$		$^1D(2p^{-1}2p^{-1})$ $k^2/2=29.611\ 57$		$^1P(2s^{-1}2p^{-1})$ $k^2/2=28.324\ 90$		$^3P(2s^{-1}2p^{-1})$ $k^2/2=28.766\ 87$	
ϵ_s	c_s	ϵ_s	c_s	ϵ_d	c_d	ϵ_p	c_p	ϵ_p	c_p
1.743 13	0.001 30	1.743 13	0.016 55	1.768 69	0.006 43	2.186 61	0.010 30	2.186 61	0.013 28
6.305 15	0.002 80	6.305 15	0.031 23	6.946 69	0.015 77	6.409 58	0.019 60	6.409 58	0.026 58
14.587 25	0.035 10	14.587 25	0.064 38	15.721 68	0.019 80	14.444 64	0.022 49	14.444 64	0.046 65
28.474 21	0.991 64	28.474 21	0.966 41	29.643 95	0.998 80	28.460 48	0.997 75	28.460 48	0.997 79
51.235 26	0.087 56	51.235 26	0.037 47	51.476 01	0.021 29	52.502 09	0.028 81	52.502 09	0.002 11
89.161 03	0.057 62	89.161 03	0.005 04	88.590 78	0.021 52	102.574 31	0.036 80	102.574 31	0.022 66
159.940 21	0.046 40	159.940 21	0.006 63	155.099 47	0.028 12	260.041 45	0.031 89	260.041 45	0.024 99

than those given in I. The reason for this is that in the present calculations we have not corrected the asymptotic behavior of the continuum orbitals through the matching procedure suggested in I. The effect of this incorrect asymptotic behavior in the coupled-channel calculations cannot be quantified exactly, and in any case, cannot be simply eliminated by scaling separately the amplitude of the various orbitals because of the presence of interference effects.

An important point, that can be seen from the results of Table III(a), is that the total Auger decay rate is quite insensitive to the inclusion of the correlation effects. This fact suggests also that the total value obtained through the coupled-channel calculations is probably underestimated by about 10%. Therefore, we conclude that the more reliable experimental value for the total Auger rate of Ne is probably that measured by Svensson *et al.* in Ref. 15.

As regards, instead, the partial decay rates obtained using the coupled-channel approach, we observe that the less satisfactory value in Tables III(a) and III(b) is that relative to the 3P final state, the partial decay rate of which is overestimated in comparison to both the Krause-Gelius^{16,17} and the Svensson¹⁵ experimental value. A possible cause of this discrepancy which is also present in the results of Howat, Aberg, and Goscinski, can be found in the fact that 3P is the only triplet among the final ionic states considered, and therefore, it is only weakly modified by the interaction with the other states,

as shown also by the small difference between independent-channel and coupled-channel results.

Moreover, we want to remark that whereas the inclusion of interchannel effects is decisive for obtaining a quantitative agreement with the experimental decay rates, its effect on the transition energies is less important and sometimes can make these quantities less close to the experimental values than the uncorrelated ones, since the correlation contributions are included only in the final states but not in the initial one. In particular, the MC-SCF calculation for the initial state changes the Hartree-Fock energy only by about 10^{-3} a.u., while the coupling between the two 1S final states enlarges their energy difference by about 4 eV instead of reducing it by 2 eV. Obviously for obtaining a better agreement with the experimental transition energies it would be necessary to take into account also “dynamic” correlation effects and relativistic energies both in the initial and in the final states. Finally, we point out that the total energy shift Δ , calculated as explained in Sec. II b, is equal to 0.096 eV, a quantity which is negligible with respect to the transition energies characteristic of the problem

B. LiF molecule

Using the method explained in Sec. II and characterized by the inclusion of the coupling among final ionic states and decay channels, we have produced a “theoretical” spectrum of the LiF molecule ionized in its deepest

TABLE II. Energies (E_{CC}) of the initial singly ionized and of the final doubly ionized state of Ne, the latter calculated using the coupled-channel approach and classified according to their hole configuration. The corresponding energy differences (ΔE_{CC}) are compared with those obtained using the independent channel approach (ΔE_{IC}) and with the experimental values (ΔE_{expt}) (Ref. 5). The energies are given in atomic units and the energy differences in electron volts.

Final states	E_{CC}	ΔE_{CC}	ΔE_{IC}	ΔE_{expt}
$^2S(1s^{-1})$	-96.626 518			
$^1S(2s^{-1}2s^{-1})$	-124.004 188	744.99	746.93	748.0±0.1
$^1P(2s^{-1}2p^{-1})$	-124.951 416	770.77	770.77	771.4±0.1
$^3P(2s^{-1}2p^{-1})$	-125.394 144	782.79	782.79	782.0±0.1
$^1S(2p^{-1}2p^{-1})$	-126.126 322	802.74	800.79	800.4±0.1
$^1D(2p^{-1}2p^{-1})$	-126.238 092	805.78	805.78	804.2±0.4

TABLE III. (a) Partial and total Auger decay rates of Ne calculated using the coupled-channel approach and starting from an initial state ($^2S:1s^{-1}$) described either by a one-configuration (Γ_{SC}) or by a many-configuration (Γ_{MC}) wave function. These values are compared with those calculated by Kelly (Γ_K) (Ref. 5) and Howat *et al.*, (Γ_H) (Ref. 6), and with the quantities (Γ_{IC}) obtained using the independent-channel approach and a one-configuration wave function for the initial state. In the last column we report the experimental values measured respectively by Krause *et al.* (Ref. 16) and Gelius *et al.* (Ref. 17) (Γ_{KG}) and by Svensson *et al.* (Ref. 15) (Γ_S). All the quantities are given in 10^{-3} atomic units. (b) Relative Auger decay rates of Ne calculated as explained in (a) and compared with those calculated by Kelly (Γ_K) and Howatt *et al.* (Γ_H), with the quantities (Γ_{IC}) obtained using the independent-channel approach and with the experimental quantities (Refs. 15–17).

(a)							
Final states	Γ_{IC}	Γ_{SC}	Γ_{MC}	Γ_K	Γ_H	Γ_{KG}	Γ_S
$^1S(2s^{-1}2s^{-1})$	0.899	0.510	0.480	0.49	0.45	0.51	0.60
$^1P(2s^{-1}2p^{-1})$	1.911	1.606	1.595	1.37	1.50	1.45	1.74
$^3P(2s^{-1}2p^{-1})$	0.732	0.740	0.719	0.49	0.70	0.53	0.63
$^1S(2p^{-1}2p^{-1})$	0.428	0.806	0.807	0.77	0.83	0.80	0.89
$^1D(2p^{-1}2p^{-1})$	5.121	5.350	5.314	4.93	5.50	5.15	6.04
Γ_{tot}	9.090	9.012	8.915	8.05	8.98	8.44±9%	9.90±9%
(b)							
Final states	Γ_{IC}	Γ_{SC}	Γ_{MC}	Γ_K	Γ_H	Γ_{expt}	
$^1S(2s^{-1}2s^{-1})$	0.176	0.095	0.090	0.099	0.082	0.099	
$^1P(2s^{-1}2p^{-1})$	0.373	0.300	0.300	0.278	0.273	0.282	
$^3P(2s^{-1}2p^{-1})$	0.143	0.138	0.135	0.099	0.127	0.103	
$^1S(2p^{-1}2p^{-1})$	0.084	0.151	0.152	0.156	0.151	0.155	
$^1D(2p^{-1}2p^{-1})$	1.000	1.000	1.000	1.000	1.000	1.000	

shell that takes into account also secondary transitions due to shakeup and shakeoff processes. In our scheme the experimental spectrum can be interpreted as originating from the superposition of three types of independent processes.

(i) The normal K - LL Auger process, in which the initial state is characterized by a single inner-shell vacancy and the final state just by two vacancies in the σ and/or π orbitals.

(ii) The shakeoff KL - LLL processes, in which the initial state, in addition to the inner-shell vacancy, is ionized in a valence orbital (4σ or 1π) and the final state is characterized by three vacancies in the σ and/or π orbitals.

(iii) The shakeup K - LL processes, in which the initial state, in addition to the inner-shell vacancy, is excited with the promotion of one electron from a valence orbital (4σ or 1π) to a virtual orbital (2π). The final state is thus characterized by three vacancies in the σ and/or π orbitals, while the excited electron remains in the 2π orbital. Note that we have not included channels in which the excited electron fills one of the three vacancies since the corresponding decay probabilities are much smaller than the others.

Following our scheme, these three processes can be treated independently, and the complete spectrum can be constructed as the superposition of three separate spectra each one characterized by their own parameters. The technical procedures used to set up this “theoretical” spectrum will be explained at the end of this section. But, as one can see from Figs. 1 and 2, our method allows

us to reproduce the experimental spectrum in a very satisfactory manner both as regards the positions and the relative intensities of the lines

Let us consider first the basis set used for our calculations. As in the case of Ne, we have utilized Hermite Gaussian functions with orbital exponents scaled in order to have eigenvectors of the average Hartree-Fock operator (20) at energies near to those of the Auger electron in the various decay channels. However, since our basis set is made up of functions centered both on F and on Li at their experimental equilibrium distance ($R = 2.955$ a.u.), we require the presence in the basis set of two distinct orbitals for each molecular symmetry, having about the same Auger energy and centered respectively on F and Li. The resulting basis set is made up of the

$$[25s (= 13s_F + 12s_{Li}) + 17p (= 10p_F + 7p_{Li}) + 8d (= 5d_F + 3d_{Li})]$$

Hermite Gaussian function and includes pairs of symmetry orbitals—at energies quite close to the Auger ones—that contribute to the expansion of the various components of the continuum orbitals in a predominant way. In what follows we will analyze separately the results obtained for the K - LL Auger transitions and for those relative to the shakeoff and shakeup processes.

1. Normal Auger transitions

In Table IV we have reported the energies and energy differences calculated with our coupled-channel approach

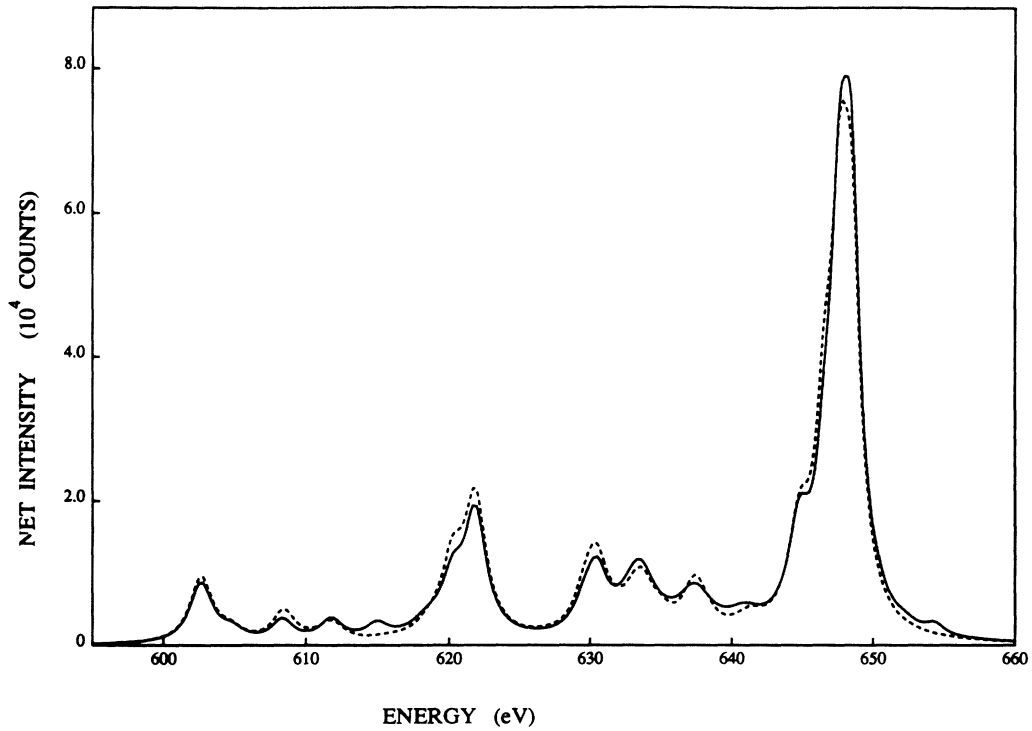


FIG. 1. Experimental Auger spectrum (—), of the LiF molecule (Ref. 18), compared with the “theoretical” one (---) constructed with the experimental linewidths.

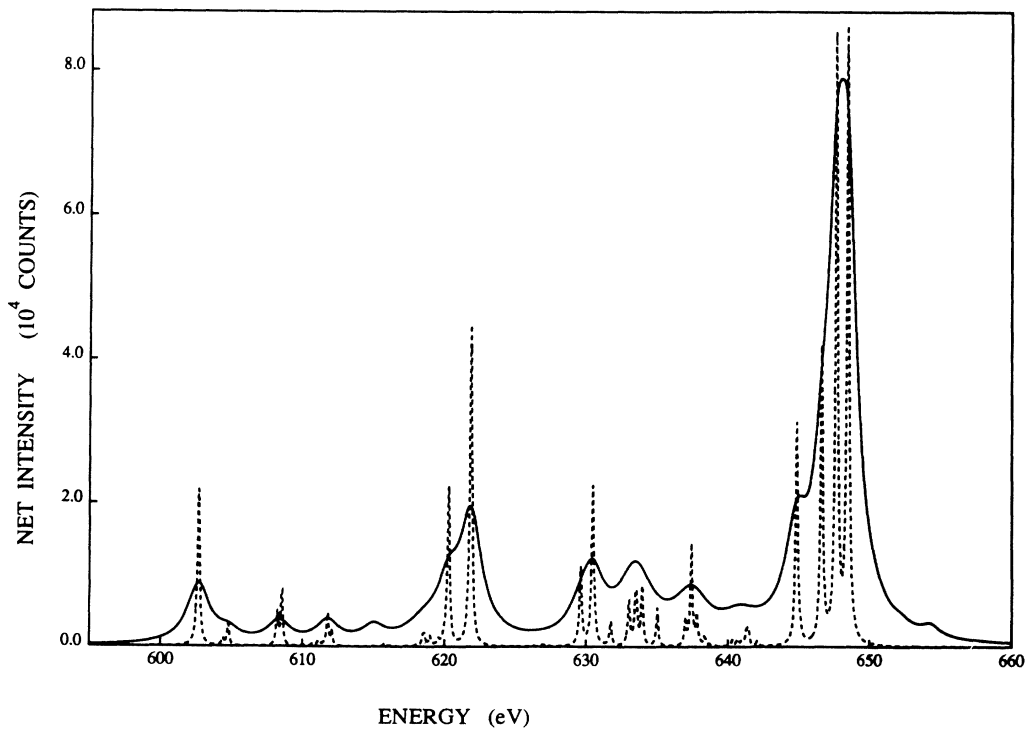


FIG. 2. Experimental Auger spectrum (—) of the LiF molecule (Ref. 18), compared with the “theoretical” one (---) constructed with the calculated linewidths.

TABLE IV. Energies (E_{CC}) of the initial singly ionized and of the final doubly ionized states of LiF, the latter calculated using the coupled-channel approach and classified according to their hole configuration. The corresponding energy differences (ΔE_{CC}) are compared with those obtained using the independent channel approach (ΔE_{IC}) and with the values (ΔE_{expt}) reported in Ref. 18. The energies are given in atomic units and the energy differences in electron volts.

Transition	Final states	E_{CC}	ΔE_{CC}	ΔE_{IC}	ΔE_{expt}
	$1\sigma^{-1};^2\Sigma^+$	-81.743 27			
1	$1\pi^{-2};^3\Sigma^-$	-105.723 28	652.53	652.53	652.2
2	$4\sigma^{-1}1\pi^{-1};^3\Pi$	-105.705 29	652.04	652.04	650.3
3	$1\pi^{-2};^1\Delta$	-105.623 01	649.81	649.81	648.5
4	$4\sigma^{-1}1\pi^{-1};^1\Pi$	-105.604 58	649.30	649.30	647.7
5	$1\pi^{-2};^1\Sigma^+$	-105.602 13	649.29	647.08	646.6
6	$4\sigma^{-2};^1\Sigma^+$	-105.518 53	646.96	647.42	644.8
7	$3\sigma^{-1}1\pi^{-1};^3\Pi$	-104.916 68	630.59	630.59	630.5
8	$3\sigma^{-1}4\sigma^{-1};^3\Sigma^+$	-104.899 27	630.11	630.11	629.6
9	$3\sigma^{-1}1\pi^{-1};^1\Pi$	-104.541 73	620.38	620.39	621.8
10	$3\sigma^{-1}4\sigma^{-1};^1\Sigma^+$	-104.523 95	619.90	619.91	620.3
11	$3\sigma^{-2};^1\Sigma^+$	-103.748 09	598.79	600.48	602.6

for 11 final ionic states representing the principal decay channels. In the same table we also report the energy differences obtained using the independent-channel approach and the experimental quantities taken from Ref. 18. We observe that the coupling among states of the same symmetry is effective only for the $^1\Sigma^+$ channels, while the energies of the others remain practically unchanged. Furthermore, we observe that the transition energies from the initial state described by a one-configuration wave function differ from the experimental values in a quantity ranging between 0 and 3.8 eV. This is due to our neglecting “dynamic” correlation effects and relativistic energies both in the initial and in the final states.

In Table V we present the absolute and relative decay rates calculated using either the coupled- or the independent-channel approach and compare these values with the experimental quantities reported in Ref. 18. Note that in the calculation of the matrix elements one

has to take into account that the orbitals of the initial state are nonorthogonal to those of the final states since they have been obtained through different SCF processes.

As for the independent-channel results, we observe that the present values are smaller (by about 10%) than those calculated in I. Essentially, this is owing to the neglect, in these calculations, of the corrections to the asymptotic behavior of the continuum orbitals. Moreover, we observe that as in the case of Ne, the total Auger rate does not change appreciably using the coupled-channel instead of the independent-channel approach. This fact also suggests that the coupled-channel value of the total decay rate is probably underestimated by about 10%. We can therefore evaluate the total Auger width as being of the order of 0.22 eV, a value similar to that measured by Svensson *et al.*¹⁵ for Ne (0.27 eV) and to that for the fluorine atom (0.1–0.2 eV),¹⁹ but considerably smaller than the widths of the deconvoluted bands reported in Ref. 18. These large observed linewidths have been attri-

TABLE V. Values of the absolute and relative Auger transition rates for LiF, calculated using the independent-channel (Γ_{IC}) and the coupled-channel (Γ_{CC}) approach and compared with the relative Auger rates ($\Gamma_{\text{expt}}^{\text{rel}}$) reported in Ref. 18. Note that the experimental value of the total Auger rate has not been clearly determined. The absolute rates are given in 10^{-3} atomic units.

Transition	Final states	Γ_{IC}^{abs}	Γ_{IC}^{rel}	Γ_{CC}^{abs}	Γ_{CC}^{rel}	$\Gamma_{\text{expt}}^{\text{rel}}$
1	$1\pi^{-2};^3\Sigma^-$	0.000	0.000	0.000	0.000	0.01
2	$4\sigma^{-1}1\pi^{-1};^3\Pi$	0.002	0.001	0.002	0.001	0.02
3	$1\pi^{-2};^1\Delta$	1.640	1.000	1.707	1.000	1.00
4	$4\sigma^{-1}1\pi^{-1};^1\Pi$	1.621	0.989	1.685	0.987	0.91
5	$1\pi^{-2};^1\Sigma^+$	0.491	0.299	0.825	0.483	0.27
6	$4\sigma^{-2};^1\Sigma^+$	0.635	0.387	0.621	0.364	0.32
7	$3\sigma^{-1}1\pi^{-1};^3\Pi$	0.437	0.267	0.442	0.259	0.20
8	$3\sigma^{-1}4\sigma^{-1};^3\Sigma^+$	0.214	0.131	0.218	0.128	0.07
9	$3\sigma^{-1}1\pi^{-1};^1\Pi$	1.029	0.627	0.899	0.526	0.42
10	$3\sigma^{-1}4\sigma^{-1};^1\Sigma^+$	0.510	0.311	0.446	0.261	0.17
11	$3\sigma^{-2};^1\Sigma^+$	0.761	0.464	0.438	0.257	0.21
Γ_{tot}			7.339		7.283	?

buted both to the dissociative character of the initial and/or final states and to the dimer formation in the target vapor.

As regards instead the partial decay rates, we point out that passing from the independent-channel to the coupled-channel results there is a clear trend in the improvement of the agreement between the calculated relative values and the corresponding "experimental" quantities given in Ref. 18. The only exception seems to be the value relative to the $(1\pi^{-2};^1\Sigma^+)$ final state. This transition, however, is very near in energy to those relative to the $(4\sigma^{-1}1\pi^{-1};^1\Pi)$ and $(4\sigma^{-2};^1\Sigma^+)$ final states. This fact makes more questionable the reliability of the corresponding quantities reported in Ref. 18 and obtained through a least-squares fit of Voigt functions to the experimental points. In fact, as pointed out also by Hotokka *et al.*,¹⁸ the decomposition of an experimental peak to the individual lines is not very accurate in cases where the lines lie near to each other (separated by an amount approximately equal to the half width of the standard line).

Finally, we point out that the calculated total energy shift Δ for the normal Auger decay process from the initial $^2\Sigma^+(1\sigma^{-1})$ state is equal to 0.083 eV, a quantity comparable to the corresponding one of Ne, but negligible if compared with the transition energies characteristic of the problem.

2. KL-LLL shakeoff processes

In Table VI we have reported the energies of four different states that can be produced when the initial ionization process not only removes an inner-shell electron, but also removes a valence electron of the molecule. The one-configuration wave functions representing the $^3\Pi$, $^3\Sigma^+$, and $^1\Pi$ states have been obtained through separate SCF calculations and their energies are upper bounds to the exact eigenvalues of the $(N-2)$ -electron Hamiltonian. The energy of the $^1\Sigma^+$ state, instead, has been calculated using a one-configuration wave function with the

same orbitals as for the $^3\Sigma^+$, since a standard SCF process, without orthogonality constraints to the lower states of the same symmetry, can produce in this case a variational collapse. Therefore, the corresponding energy is only a rough estimate of the "exact" one. Furthermore, the decay rates calculated using this approximate representation of the $^1\Sigma^+$ state are less reliable than those of the other states. In the same table we have also reported the total energy shifts for the four initial states produced by shakeoff processes: all these quantities are approximately of the same order of magnitude, but negligible with respect to the characteristic energies of the problem.

In Table VII we present the absolute and relative decay rates for various final ionic states produced by shakeoff processes. These quantities, together with the corresponding transition energies, have been calculated using the coupled-channel approach and starting from the four initial states given in Table VI. We observe that the transition energies are distributed in two different regions.

(i) 630–640 eV, where the final-state hole configurations are $(4\sigma^{-1}1\pi^{-2})$, $(4\sigma^{-2}1\pi^{-1})$, and $(1\pi^{-3})$, and the most intense peaks are around 632–633 eV and 635–637 eV.

(ii) 603–620 eV, where the final-state hole configurations are $(3\sigma^{-1}1\pi^{-2})$, $(3\sigma^{-1}4\sigma^{-1}1\pi^{-1})$, and $(3\sigma^{-1}4\sigma^{-2})$, and the most intense peaks are around 602–603 eV and 606–611 eV.

In Ref. 18 only a few of these transitions have been identified and, among these, the $[(1\sigma^{-1}1\pi^{-1};^1,^3\Pi) \rightarrow (1\pi^{-3};^2\Pi)]$ ones have been located at energies ($\Delta E = 637.76$ and 633.87 eV) very similar to those given by us in Table VII. As regards instead the $[(1\sigma^{-1}1\pi^{-1});^1,^3\Pi \rightarrow (3\sigma^{-1}1\pi^{-2};^2,^4\Sigma, ^2,^4\Delta)]$ transitions between 602 and 610 eV, we observe that, while the two final $^2\Sigma$ states reported in Table IV of Ref. 18 at $\Delta E = 606.14$ and 602.25 eV can be identified with the two $^2\Sigma^-$ states of our Table VII ($\Delta E = 606.74$ and 603.26 eV), the tentative assignment of the other final states $^4\Sigma$, $^2\Delta$ and $^2\Delta$, proposed in Ref. 18 at energies $\Delta E = 609.38$, 606.01 , and 602.11 eV, is in complete disagreement with

TABLE VI. Energies (E) and energy shifts (Δ) of initial states of LiF produced by shakeoff and shakeup processes and classified according to their hole configuration. Note that for the shakeup processes only the calculated energy shifts are given in the last column. States having the same symmetry have been coupled, the energies are given in atomic units and the energy shifts in electron volts.

States	Shakeoff		States	Shakeup	
	E	Δ		E	Δ
Hole configuration: $1\sigma^{-1}4\sigma^{-1}$			Hole configuration: $1\sigma^{-1}1\pi^{-1}$		
1 $^3\Sigma^+$	-80.683 69	0.081	1 $^4\Sigma^+$	-81.039 33	0.071
2 $^1\Sigma^+$	-80.554 46	0.080	2 $^4\Delta$	-81.033 77	0.051
Hole configuration: $1\sigma^{-1}1\pi^{-1}$			3 $^2\Delta$	-81.028 51	
3 $^3\Pi$	-80.700 85	0.065	4 $^4\Sigma^-$	-81.028 22	
4 $^1\Pi$	-80.573 12	0.067	5 $^2\Sigma^-$	-81.025 87	
			6 $^2\Sigma^+$	-81.011 23	0.071
			7 $^2\Delta$	-80.908 85	
			8 $^2\Sigma^-$	-80.904 25	
			9 $^2\Sigma^+$	-80.904 06	

TABLE VII. Transition energies (ΔE) and absolute and relative values of the particle decay rates (Γ) for various final ionic states produced by four different shakeoff processes. The states are classified according to their hole configuration, the energies are given in electron volts, and the decay rates in 10^{-3} atomic units.

Initial state		$1\sigma^{-1}4\sigma^{-1};^3\Sigma^+$			$1\sigma^{-1}4\sigma^{-1};^1\Sigma^+$		
Final states	ΔE	Γ_{abs}	Γ_{rel}	ΔE	Γ_{abs}	Γ_{rel}	
1	$4\sigma^{-1}1\pi^{-2};^2\Delta$	633.94	2.128	1.000	637.46	2.122	1.000
2	$4\sigma^{-1}1\pi^{-2};^2\Sigma^+$	632.21	0.850	0.399	635.73	0.848	0.400
3	$4\sigma^{-2}1\pi^{-1};^2\Pi$	632.02	1.063	0.500	635.53	1.065	0.502
4	$3\sigma^{-1}4\sigma^{-1}1\pi^{-1};^4\Pi$	619.31	0.440	0.206	622.83	0.000	0.000
5	$3\sigma^{-1}4\sigma^{-1}1\pi^{-1};^2\Pi$	611.00	0.545	0.256	614.52	0.008	0.004
6	$3\sigma^{-1}4\sigma^{-2};^2\Sigma^+$	609.07	0.537	0.252	612.59	0.015	0.007
7	$3\sigma^{-1}4\sigma^{-1}1\pi^{-1};^2\Pi$	603.32	0.602	0.283	606.83	1.621	0.764
8	$3\sigma^{-2}4\sigma^{-1};^2\Sigma^+$	585.15	0.547	0.257	588.67	0.608	0.287
Γ_{tot}		6.712			6.287		
Initial state		$1\sigma^{-1}1\pi^{-1};^3\Pi$			$1\sigma^{-1}1\pi^{-1};^1\Pi$		
Final states	ΔE	Γ_{abs}	Γ_{rel}	ΔE	Γ_{abs}	Γ_{rel}	
1	$4\sigma^{-1}1\pi^{-2};^4\Sigma^-$	637.95	0.001	0.001	641.43	0.000	0.000
2	$1\pi^{-3};^2\Pi$	633.57	1.458	1.000	637.05	1.366	1.000
3	$4\sigma^{-1}1\pi^{-2};^2\Delta$	633.47	0.531	0.364	636.95	0.510	0.374
4	$4\sigma^{-1}1\pi^{-2};^2\Sigma^-$	633.47	0.795	0.545	636.95	0.774	0.566
5	$4\sigma^{-2}1\pi^{-1};^2\Pi$	631.66	1.004	0.689	635.13	0.985	0.721
6	$4\sigma^{-1}1\pi^{-2};^2\Sigma^+$	630.50	0.269	0.184	633.97	0.258	0.189
7	$3\sigma^{-1}1\pi^{-2};^4\Sigma^-$	619.27	0.225	0.154	622.75	0.000	0.000
8	$3\sigma^{-1}4\sigma^{-1}1\pi^{-1};^4\Pi$	618.85	0.214	0.147	622.33	0.000	0.000
9	$3\sigma^{-1}1\pi^{-2};^2\Delta$	610.96	0.554	0.380	614.44	0.007	0.005
10	$3\sigma^{-1}4\sigma^{-1}1\pi^{-1};^2\Pi$	610.53	0.264	0.181	614.01	0.007	0.005
11	$3\sigma^{-1}1\pi^{-2};^2\Sigma^+$	607.98	0.271	0.186	611.46	0.004	0.003
12	$3\sigma^{-1}1\pi^{-2};^2\Sigma^-$	603.26	0.302	0.207	606.74	0.762	0.558
13	$3\sigma^{-1}4\sigma^{-1}1\pi^{-1};^2\Pi$	602.86	0.292	0.200	606.34	0.807	0.591
14	$3\sigma^{-2}1\pi^{-1};^2\Pi$	585.06	0.542	0.372	588.54	0.620	0.454
Γ_{tot}		6.722			6.101		

our results of Table VII. In this regard, we think that only from the simultaneous analysis of all the main possible decay states classified according to their spin and spatial symmetries can a reliable assignment of the various experimental transitions become possible.

3. *K-LL shakeup processes*

In Table VI we have reported the energies and energy shifts of nine different states that can be produced when the initial process not only removes an inner-shell electron of the molecule, but also promotes a valence electron into a 2π orbital. The one-configuration wave functions representing the various initial states have been constructed using orbitals which are eigenfunctions of an average Hartree-Fock operator and their energy shifts calculated as explained in Sec. II B.

In Tables VIII and IX we present the absolute and relative decay rates for final ionic states produced by shakeup processes. These quantities, together with the corresponding transition energies, have been calculated using the coupled-channel approach and starting from three of the nine initial states given in Table VI.

First of all, we observe that the total decay rates from the $^4\Sigma^+$ and the $^2\Sigma^+$ states are practically identical. This fact suggests that probably the same is also true for the remaining Σ states of Table VI, and also that the two $^2\Delta$

states should have the same total decay rates as $^4\Delta$, the calculated value of which is given in Table IX. This assumption has been used in the construction of the “theoretical” spectrum shown in Figs. 1 and 2.

Furthermore we observe that the transition energies are distributed in two different regions.

(i) 635–646 eV, where the final-state hole configurations are $(4\sigma^{-1}1\pi^{-2})$, $(4\sigma^{-2}1\pi^{-1})$, and $(1\pi^{-3})$, and the most intense peaks are around 638 and 640–642 eV.

(ii) 609–628 eV, where the final-state hole configurations are $(3\sigma^{-1}1\pi^{-2})$ and $(3\sigma^{-1}4\sigma^{-1}1\pi^{-1})$, and the most intense peaks are around 611–618 eV.

In Ref. 18 only two possible transitions have been calculated (both around 641 eV) and identified with the $[(1\sigma^{-1}1\pi^{-1});^2\Sigma \rightarrow (1\pi^{-3};^1,^3\Sigma)]$ ones. In Tables VIII and IX we report several other transitions in this energy region, besides the previous two, and they all together produce a small peak in the “theoretical” spectrum around 641 eV (see Figs. 1 and 2).

As regards instead the experimental peak around 615 eV, in spite of the presence of non-negligible transitions between 611 and 618 eV owing to both shakeup and of shakeoff processes, we are not able to obtain a peak in the “theoretical” spectrum around 615 eV: a possible explanation of this fact is that we have missed a different type of decay process in this part of the spectrum. Final-

TABLE VIII. Transition energies (ΔE) and absolute and relative values of the partial decay rates (Γ) for various final ionic states produced by two different shakeup processes in which one electron has been promoted to the 2π orbital. The states are classified according to their hole configuration, the energies are given in electron volts, and the decay rates in 10^{-3} atomic units.

Initial state Final states	ΔE	$1\sigma^{-1}1\pi^{-1,4}\Sigma^+$		ΔE	$1\sigma^{-1}1\pi^{-1,2}\Sigma^+$	
		Γ_{abs}	Γ_{rel}		Γ_{abs}	Γ_{rel}
1 $4\sigma^{-1}1\pi^{-2,5}\Pi$	645.73	0.001	0.001	646.49	0.000	0.000
2 $4\sigma^{-1}1\pi^{-2,3}\Pi$	644.93	0.005	0.005	645.70	0.002	0.004
3 $1\pi^{-3,3}\Sigma^+$	641.33	0.607	0.571	642.09	0.233	0.373
4 $4\sigma^{-1}1\pi^{-2,3}\Pi$	641.27	1.063	1.000	642.04	0.412	0.659
5 $4\sigma^{-1}1\pi^{-2,3}\Pi$	640.65	0.064	0.060	641.41	0.026	0.042
6 $1\pi^{-3,1}\Delta$	640.64	0.000	0.000	641.40	0.290	0.465
7 $1\pi^{-3,3}\Delta$	640.32	0.847	0.797	641.08	0.318	0.509
8 $4\sigma^{-1}1\pi^{-2,1}\Pi$	639.96	0.000	0.000	640.72	0.625	1.000
9 $1\pi^{-3,1}\Sigma^+$	639.85	0.000	0.000	640.61	0.339	0.543
10 $4\sigma^{-2}1\pi^{-1,3}\Sigma^+$	638.32	0.280	0.264	639.09	0.118	0.189
11 $4\sigma^{-1}1\pi^{-2,3}\Pi$	638.09	0.190	0.179	638.85	0.074	0.119
12 $4\sigma^{-1}1\pi^{-2,1}\Pi$	637.94	0.000	0.000	638.70	0.228	0.365
13 $4\sigma^{-2}1\pi^{-1,1}\Delta$	637.68	0.000	0.000	638.44	0.235	0.377
14 $4\sigma^{-2}1\pi^{-1,1}\Sigma^+$	636.59	0.000	0.000	637.35	0.240	0.384
15 $3\sigma^{-1}1\pi^{-2,5}\Pi$	627.14	0.150	0.141	627.90	0.000	0.000
16 $3\sigma^{-1}4\sigma^{-1}1\pi^{-1,5}\Sigma^+$	626.90	0.156	0.147	627.66	0.000	0.000
17 $3\sigma^{-1}1\pi^{-2,3}\Pi$	626.15	0.010	0.010	626.97	0.134	0.215
18 $3\sigma^{-1}4\sigma^{-1}1\pi^{-1,3}\Sigma^+$	625.39	0.019	0.018	626.15	0.151	0.241
19 $3\sigma^{-1}1\pi^{-2,3}\Pi$	618.44	0.487	0.458	619.16	0.132	0.211
20 $3\sigma^{-1}1\pi^{-2,1}\Pi$	618.21	0.000	0.000	618.97	0.302	0.483
21 $3\sigma^{-1}4\sigma^{-1}1\pi^{-1,3}\Sigma^+$	618.05	0.246	0.231	618.82	0.081	0.129
22 $3\sigma^{-1}4\sigma^{-1}1\pi^{-1,1}\Sigma^+$	617.94	0.000	0.000	618.70	0.136	0.218
23 $3\sigma^{-1}1\pi^{-2,3}\Pi$	615.71	0.232	0.218	616.46	0.060	0.096
24 $3\sigma^{-1}1\pi^{-2,1}\Pi$	615.49	0.000	0.000	616.22	0.132	0.211
25 $3\sigma^{-1}1\pi^{-2,3}\Pi$	611.07	0.010	0.010	611.83	0.117	0.188
26 $3\sigma^{-1}4\sigma^{-1}1\pi^{-1,3}\Sigma^+$	610.68	0.295	0.278	611.45	0.119	0.191
27 $3\sigma^{-1}1\pi^{-2,1}\Pi$	610.29	0.000	0.000	611.05	0.216	0.346
28 $3\sigma^{-1}4\sigma^{-1}1\pi^{-1,1}\Sigma^+$	609.30	0.000	0.000	610.06	0.191	0.305
Γ_{tot}		4.918			4.910	

ly, we point out that the small peak around 654 eV lies outside the energy region considered in this article.

4. Construction of the “theoretical” spectrum

An important point that emerges from the comparison between calculated and experimental quantities is that in our method the predicted values of the decay rates are more accurate than those of the transition energies. This characteristic is an obvious consequence of the fact that our method neglects both the “dynamic” correlation effects and the relativistic corrections to the energies of the initial and final states. Our calculations show that there is an uncertainty in the transition energies of the order of ± 2 eV around the values calculated in the coupled-channel approach and in order to reduce this uncertainty the use of a strongly correlated wave functions would be necessary.

A simple way for avoiding this difficulty and obtaining equally an accurate fit of the experimental spectrum is to construct a “theoretical” Auger spectrum through the following superposition of Lorentzians:

$$S_{\text{A}}^{\text{theor}}(E) = c_{\text{A}} \sum_i \frac{\Gamma_i/2}{(E - E_i)^2 + \Gamma_{\text{A}}^2/4}, \quad (45)$$

where Γ_i and Γ_{A} are the partial and total Auger decay rates calculated with our method, c_{A} is a scaling constant, and $\{E_i\}$ the resonance energies that can be used as empirical parameters to fit the experimental spectrum by allowing small changes around the calculated values. In a similar way one can proceed also for the shakeoff and shakeup spectra, so that the final “theoretical” spectrum to be compared with the experimental one is the following:

$$S_{\text{A}}^{\text{theor}}(E) = c_{\text{A}} \sum_i \frac{\Gamma_i/2}{(E - E_i)^2 + \Gamma_{\text{A}}^2/4} + \sum_{j=1}^{\text{SO}} c_j \sum_i \frac{\Gamma_{ij}/2}{(E - E_{ij})^2 + \Gamma_j^2/4} + \sum_{j=1}^{\text{SU}} c_j \sum_i \frac{\Gamma_{ij}/2}{(E - E_{ij})^2 + \Gamma_j^2/4}. \quad (46)$$

The scale constants (c_{A} , c_j^{SO} , and c_j^{SU}), which are as many as initial states of Auger, shakeoff, and shakeup processes, have been used as empirical parameters optimized by requiring that the total integrated intensity be equal to that of the experimental spectrum. This one has been reconstructed by superposing 20 Lorentzians with

TABLE IX. Transition energies (ΔE) and absolute and relative values of the partial decay rates (Γ) for various final ionic states produced by a shakeup process in which one electron has been promoted to the 2π orbital. The states are classified according to their hole configuration, the energies are given in electron volts, and the decay rates in 10^{-3} atomic units.

Initial state	Final states	ΔE	$1\sigma^{-1}1\pi^{-1,4}\Delta$ Γ_{abs}	Γ_{rel}
1	$4\sigma^{-1}1\pi^{-2,5}\Pi$	645.88	0.001	0.001
2	$4\sigma^{-1}1\pi^{-2,3}\Pi$	645.09	0.004	0.007
3	$1\pi^{-3,3}\Delta$	641.49	0.583	1.000
4	$1\pi^{-3,3}\Sigma^+$	641.48	0.271	0.464
5	$4\sigma^{-1}1\pi^{-2,3}\Phi$	641.38	0.448	0.769
6	$1\pi^{-3,3}\Sigma^-$	640.99	0.275	0.472
7	$4\sigma^{-1}1\pi^{-2,3}\Pi$	640.80	0.106	0.181
8	$4\sigma^{-2}1\pi^{-1,3}\Sigma^+$	638.46	0.175	0.300
9	$4\sigma^{-2}1\pi^{-1,3}\Delta$	638.34	0.346	0.593
10	$4\sigma^{-2}1\pi^{-1,3}\Sigma^-$	637.95	0.166	0.286
11	$3\sigma^{-1}1\pi^{-2,3}\Pi$	627.29	0.152	0.260
12	$3\sigma^{-1}4\sigma^{-1}1\pi^{-1,3}\Delta$	626.36	0.011	0.018
13	$3\sigma^{-1}1\pi^{-2,3}\Pi$	626.35	0.006	0.010
14	$3\sigma^{-1}1\pi^{-2,3}\Phi$	618.97	0.425	0.730
15	$3\sigma^{-1}4\sigma^{-1}1\pi^{-1,3}\Delta$	618.44	0.227	0.390
16	$3\sigma^{-1}1\pi^{-2,3}\Pi$	615.85	0.204	0.349
17	$3\sigma^{-1}1\pi^{-2,3}\Pi$	611.22	0.271	0.465
	Γ_{tot}		3.671	

intensities and linewidths taken from Table I of Ref. 18.

The final results of these procedures are reported in Fig. 1 in which we compare the experimental and theoretical spectra. Note that to make this comparison more consistent, we have used in Eq. (46) the experimen-

tal linewidths (Γ_A , Γ_{SO} and Γ_{SU}) taken from Table I of Ref. 18 instead of those we have calculated which are different because of the presence in the experimental spectrum of other sources of line broadening (see comments on the linewidth of the normal Auger transitions).

An important result from this procedure is that, in our theoretical spectrum, the integrated intensity of the satellite lines gives about 23% of the total one, a value very close to that (25%) reported in Ref. 18. In particular, the shakeoff processes contribute 18% while the remaining 5% is due to the shakeup processes.

Finally, to display more clearly the details of the spectrum hidden in Fig. 1 by extrinsic line broadenings, we have plotted in Fig. 2 a theoretical spectrum obtained from Eq. (46) using the calculated linewidths which are given in Tables V, VII, VIII and IX. Note that for the arbitrary constants (c_A , c_j^{SO} , and c_j^{SU}) we have used the same values as in Fig. 1 divided by 4 for scale reasons.

To conclude, we observe that our method allows us to reproduce quite precisely the main features of the experimental spectrum. The remaining discrepancies can be attributed both to the intrinsic limitations of the method (no correlation contributions to the initial state, no relativistic energies, incorrect asymptotic behavior of the continuum orbitals, no coupling between electronic and nuclear motion, etc.) and to the fact that a few decay mechanisms have not been taken into account; for example, the $1\sigma^{-1}3\sigma^{-1}$ shakeoff and $3\sigma^{-2}1\pi^{-1}2\pi$ shakeup processes.

ACKNOWLEDGMENTS

One of us (S.S.) wishes to acknowledge the financial support granted by ENI (Ente Nazionale Idrocarburi) within the "Perfezionamento in Scienze Molecolari Applicate" at Scuola Normale Superiore.

¹R. Colle and S. Simonucci, Phys. Rev. A **39**, 6247 (1989).

²R. Colle and S. Simonucci, Nuovo Cimento D **11**, 1587 (1989).

³R. Colle and S. Simonucci, in *Progress on Electronic Properties of Solids*, edited by R. Girlanda *et al.* (Kluwer, Amsterdam, 1989), p. 211.

⁴R. Colle and O. Salvetti, in *Density Matrices and Density Functionals*, Proceedings of the Second International Congress of Quantum Chemistry, edited by R. Erdhal and V. H. Smith, Jr. (Reidel, Dordrecht, 1987), and references therein.

⁵H. P. Kelly, Phys. Rev. A **11**, 556 (1975).

⁶G. Howat, T. Aberg, and O. Goscinski, J. Phys. B **11**, 1575 (1978).

⁷R. Colle, S. Simonucci, and T.O. Woodruff, Phys. Rev. A **38**, 694 (1988).

⁸W. Sander, in *Proceedings of the 15th International Conference on the Physics of Electronic and Atomic Collisions, Brighton, 1987*, edited by H. G. Gilbody, W. R. Newell, F. H. Read, and A. C. H. Smith (Plenum, New York, 1988), and references therein.

⁹U. Fano, Phys. Rev. **124**, 1866 (1961).

¹⁰T. Aberg and G. Howat, in *Corpuscles and Radiation in Matter I*, Vol. 31 of *Handbuch der Physik*, edited by S. Flügge (Springer, Berlin, 1982), and references therein.

¹¹A. Golebiewski and J. Mrozek, Int. J. Quantum Chem. **7**, 263 (1973); **7**, 1021 (1973).

¹²J. C. Phillips and L. Kleimann, Phys. Rev. **116**, 287 (1959).

¹³R. Colle, A. Fortunelli, and S. Simonucci, Nuovo Cimento D **9**, 969 (1987).

¹⁴R. Colle, A. Fortunelli, and S. Simonucci, Nuovo Cimento D **10**, 805 (1988).

¹⁵S. Svensson, N. Martensson, E. Basilier, P. A. Malmqvist, U. Gelius, and K. Siegbahn, Phys. Scr. **14**, 141 (1976).

¹⁶M. O. Krause, F. A. Stevie, L. J. Lewis, T. A. Carlson, and W. E. Moddeman, Phys. Rev. Lett. A **31**, 91 (1970).

¹⁷U. Gelius, S. Svensson, H. Siegbahn, E. Basilier, A. Faxalv, and K. Siegbahn, Chem. Phys. Lett. **28**, 1 (1974).

¹⁸M. Hotokka, H. Ågren, H. Aksela, and S. Aksela, Phys. Rev. A **30**, 1855 (1984).

¹⁹O. Goscinski, J. Müller, E. Poulain, and H. Siegbahn, Chem. Phys. Lett. **55**, 407 (1978).